Supplemental material for:

Swallow E.J., Wilson C.J.N., Charlier B.L.A., and Gamble, J.A. (2018)

Mafic inputs into the rhyolitic magmatic system of the 2.08 Ma Huckleberry Ridge eruption, Yellowstone.

American Mineralogist 103 (5), doi.org/10.2138/am-2018-6273

List of files accompanying the manuscript as online supplemental materials.
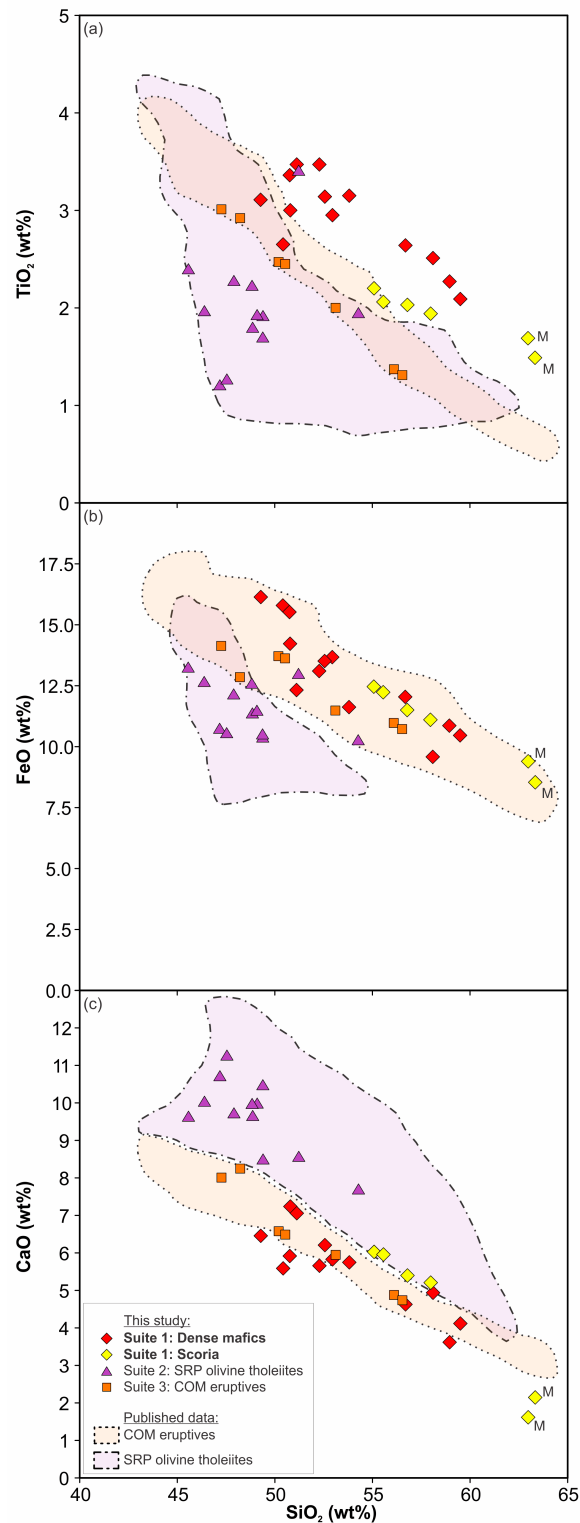
1. Supplemental material

- Cover page and contents listing
- Supplemental Table 1: Table documenting samples analyzed in this study.
- Supplemental Fig. 1: SiO_2 vs. (a) TiO_2, (b) FeO and (c) CaO for the three suites analyzed in this study and relevant fields of published data.
- Supplemental Fig. 2: SiO_2 vs. (a) Rb, (b) Sr and (c) V for the suites analyzed in this study and relevant fields of published data.
- Supplemental Fig. 3: Ce/Pb vs. Zr/Hf for the suites analyzed in this study and relevant fields of published data.
- Supplemental Fig. 4: SiO_2 plotted against (a) K/Rb and (b) K/Ba values for all the suites in this study and fields from published data.
- Supplemental Fig. 5: Pb-Pb isochrons generated using Isoplot.
- Supplemental Fig. 6: Ba/Nb vs. Nb/Zr for all suites in this study.
- Supplemental Fig. 7: Sr isotope isochron generated using Isoplot.
- Supplemental Fig. 8: Plots showing the relationship between MgO, CaO/Al_2O_3 and Ni/Sc, showing intra-suite variation.
- Supplemental Fig. 9: Ni/Cr vs. Sr/Sc ratios for the samples analyzed in this study.
- Isotope methodologies

Electronic appendix 1: Full major and trace elemental concentrations, and isotopic ratios for the samples analyzed in this study.
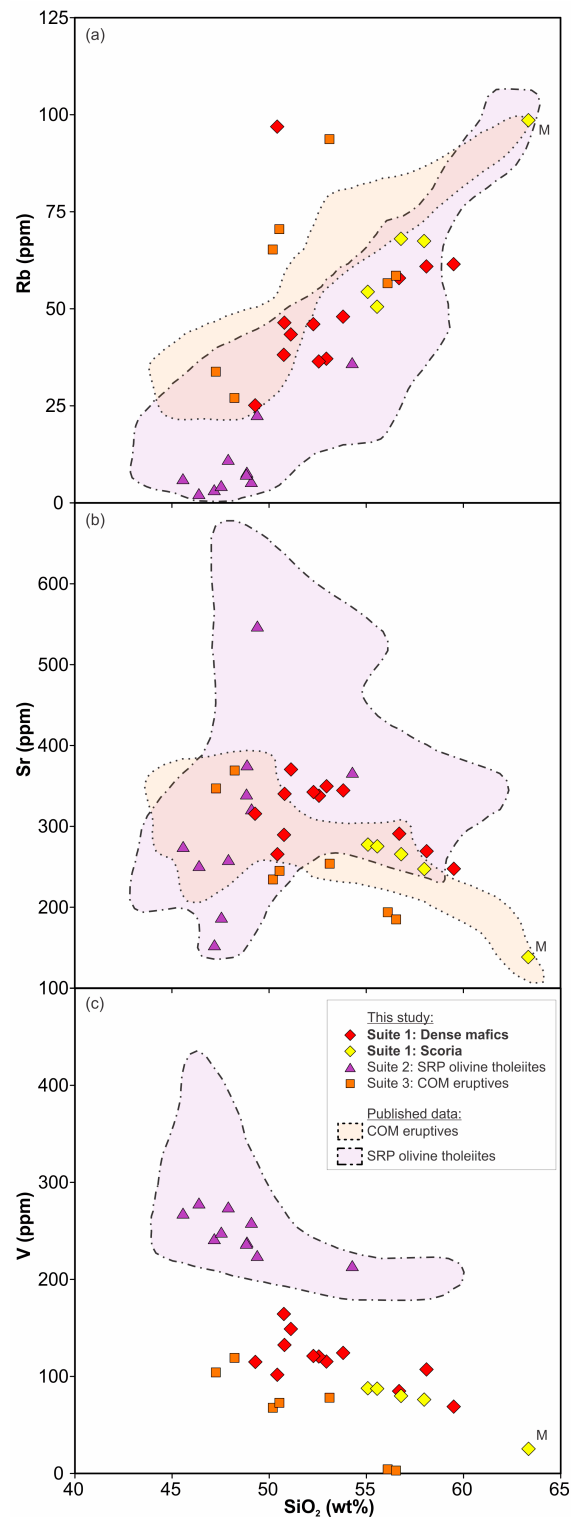
Electronic appendix 2: Table of published data from GEOROC database (http://georoc.mpch-mainz.gwdg.de/georoc/) which met compositional criteria.

Supplemental Table 1: Table documenting samples analyzed in this study for each mafic suite listed in Table 1.
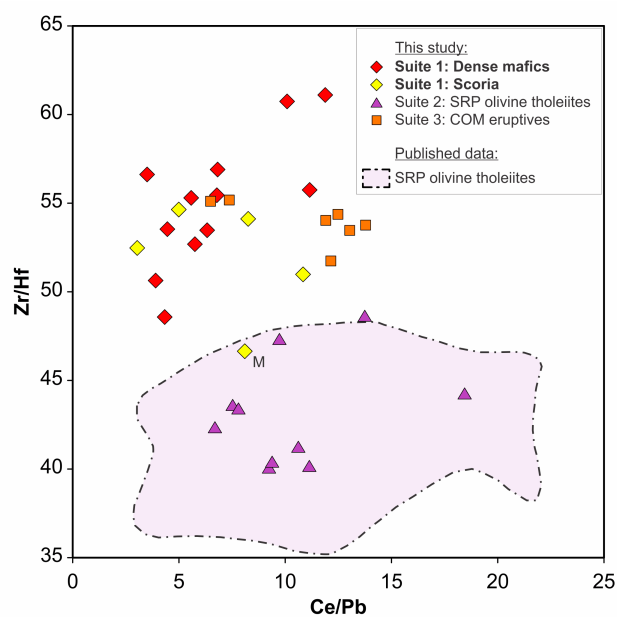
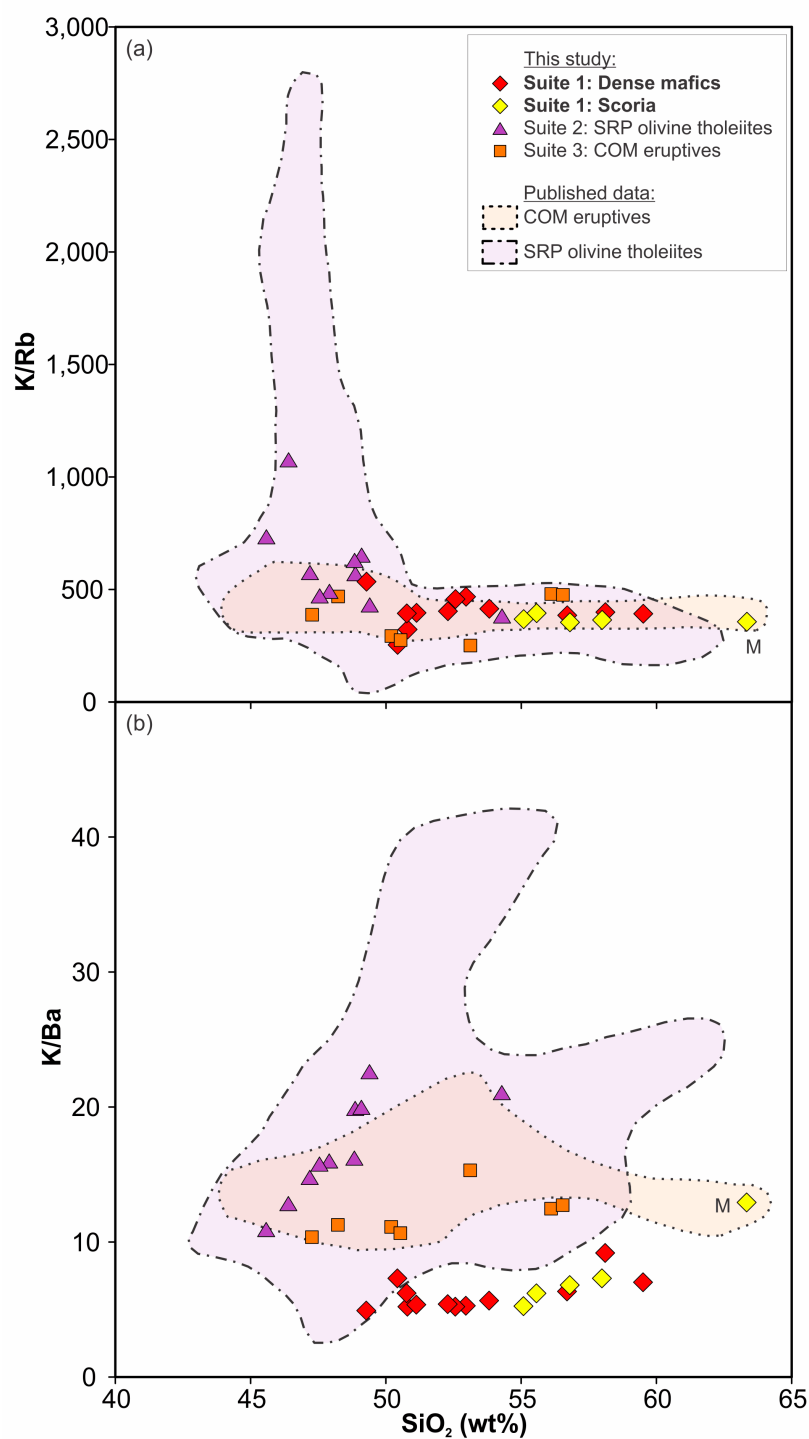| Sample type	Sample ID	Locality (UTM zone 12), easting, northing	Host HRT member or eruptive unit
Suite 1: dense mafics	YP122	456848, 4877524	(A)
	YP243	454137, 4890366	(A)
	YP244	454137, 4890366	(A)
	YP246	454137, 4890366	(A)
	YP248	454137, 4890366	(A)
	YP381	464771, 4884027	(A)
	YP382	464771, 4884027	(A)
	YP383	464771, 4884027	(A)
	YP384	464646, 4884097	(A)
	YP385	464646, 4884097	(A)
	YP447	464646, 4884097	(A)
	YP448	464771, 4884027	(A)
	YP449	464771, 4884027	(A)
	YP242	452598, 4889036	(B)
Suite 1: scoria	YP185	476874, 4887036	(A)
	YP188	476874, 4887036	(A)
	YP071BLACK	451507, 4864635	(B)
	YP071RED	451507, 4864635	(B)
	YP266SCORIA	451394, 4864614	(B)
	YP334B	451507, 4864635	(B)
	YP083SCORIA	451507, 4864635	(B)
Suite 2	YR289	471761, 4878361	Falls River Basalt
	YR291	476651, 4885380	Warm River Basalt
	YR292	548102, 4972327	Basalt of the Narrows (topmost lava)
	YR294	548397, 4974082	Junction Butte Basalt (Junction Butte)
	YR296	536172, 4978238	Undine Falls Basalt (Gardiner River)
	YR297	530622, 4977997	Junction Butte Basalt (north of Blacktail Deer ponds)
	YR300	511629, 4943650	Madison Basalt (Madison Junction)
	YR302	468222, 4915236	Gerrit Basalt (Henrys Fork river)
	YR303	455860, 4903130	Snake River Basalt
	YR307	474598, 4892348	Gerrit Basalt
	YR327	458439, 4863208	Junction Butte Basalt (beneath HRT in diapirically upheaved rocks)
	YR362	547838, 4975353	Junction Butte Basalt (Tower Creek)
Suite 3	YR304	455497, 4901523	High Point scoria cone
	YR305	455510, 4901472	High Point scoria cone
	YR418	448232, 4905177	Un-named scoria cone
	YR420	448232, 4905177	Un-named scoria cone
	YR421	445780, 4904771	Fogg Butte
	YR422	444627, 4904086	Crystal Butte
	YR425	434543, 4905055	Blacks Knoll

Supplemental Fig. 1: SiO_2 vs. (a) TiO_2, (b) FeO and (c) CaO for the three suites analyzed in this study and relevant fields of published data (see text in the main paper for sources of published data). Plots show elevated TiO_2 and FeO, and lower CaO in Suites 1 and 3 relative to Suite 2. Suite 1 is distinct by its higher TiO_2 compared to all suites and published data from COM eruptives. 2sd uncertainties are smaller than the symbol size.

Supplemental Fig. 2: SiO_2 vs. (a) Rb, (b) Sr and (c) V for the suites analyzed in this study and relevant fields of published data (see text in the main paper for sources of published data). Plots show higher Rb in Suites 1 and 3 compared to Suite 2 for a given value of SiO_2 but Sr is comparable between the different suites. Suite 2 is enriched in V. 2sd uncertainties are smaller than the symbol size.
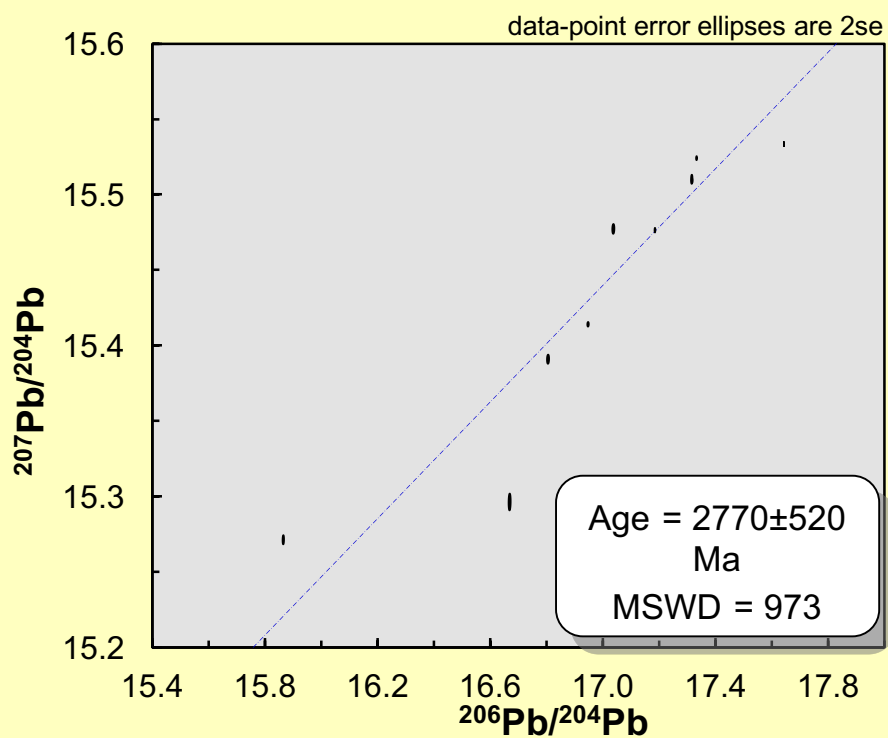
Supplemental Fig. 3: Ce/Pb vs. Zr/Hf for the suites analyzed in this study and relevant fields of published data (see text in the main paper for sources of published data). Due to the similar partition coefficients between both elements in each ratio, ratios should be uniform. Although Ce/Pb ratios are similar for all suites, Suite 1 and 3 samples show elevated Zr/Hf ratios.
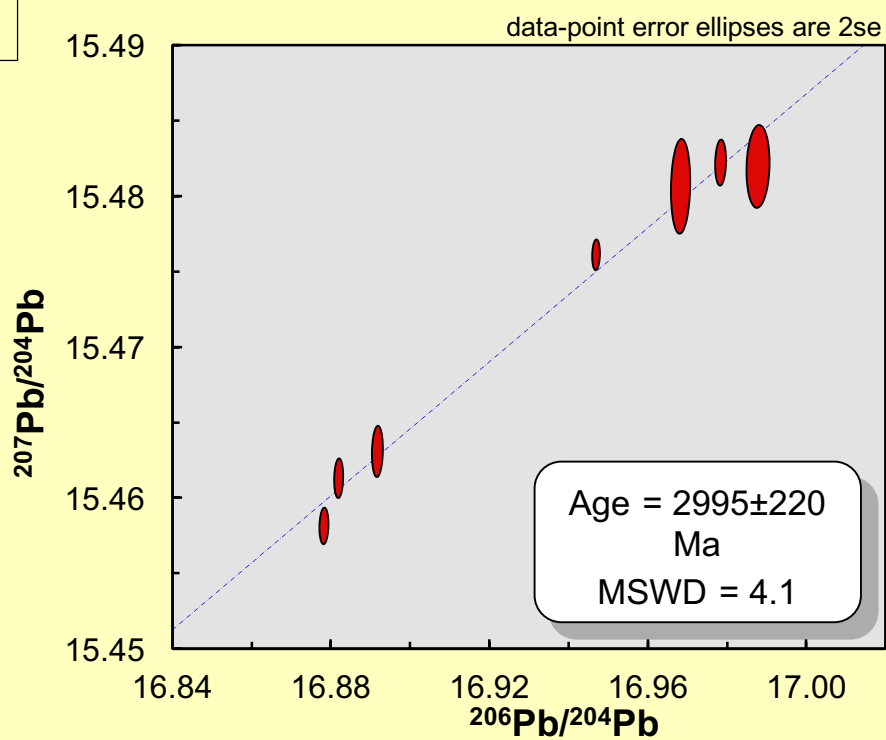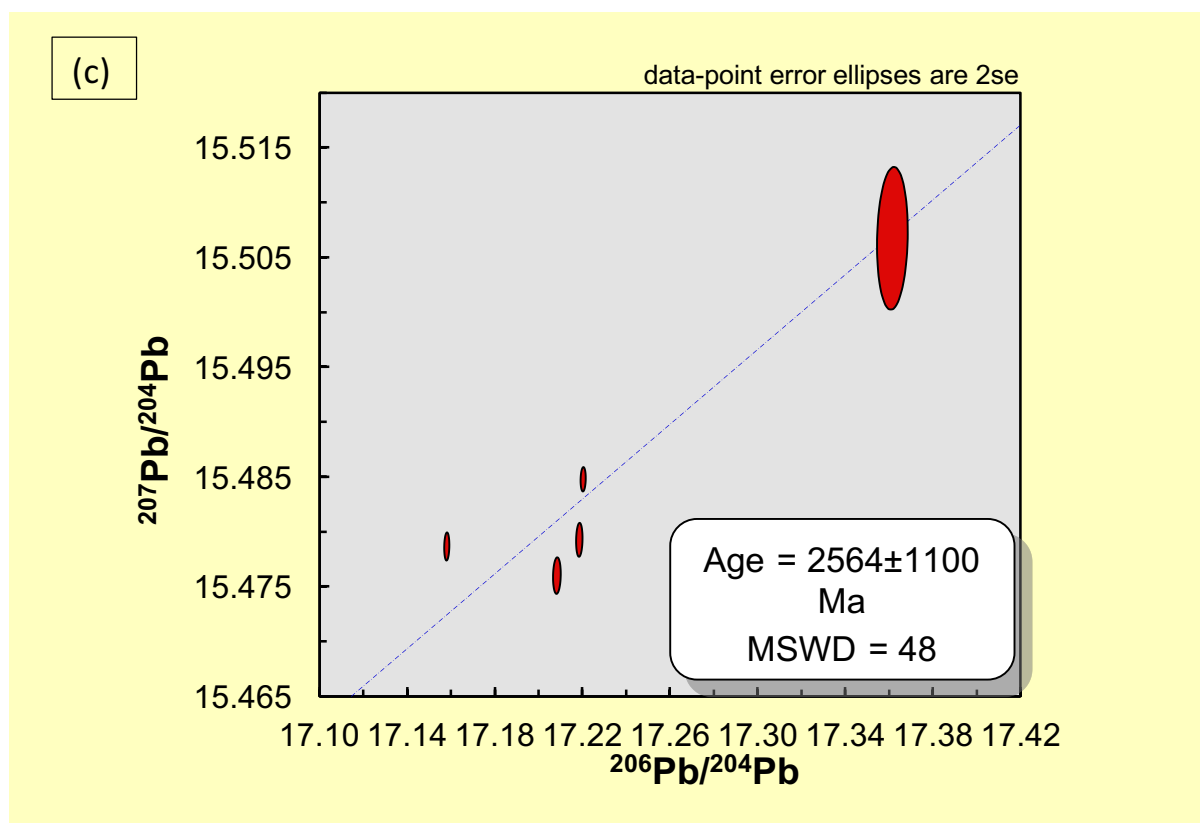
Supplemental Fig. 4: SiO_2 plotted against (a) K/Rb and (b) K/Ba values for all the suites in this study and fields from published data (see text in the main paper for sources). Ratios would would likely strongly increase and decrease, respectively, with crustal contamination. The uniformity or weakly positive slopes in Suite 1 samples indicates the inter- and intra-suite variation is not controlled by crustal contamination.
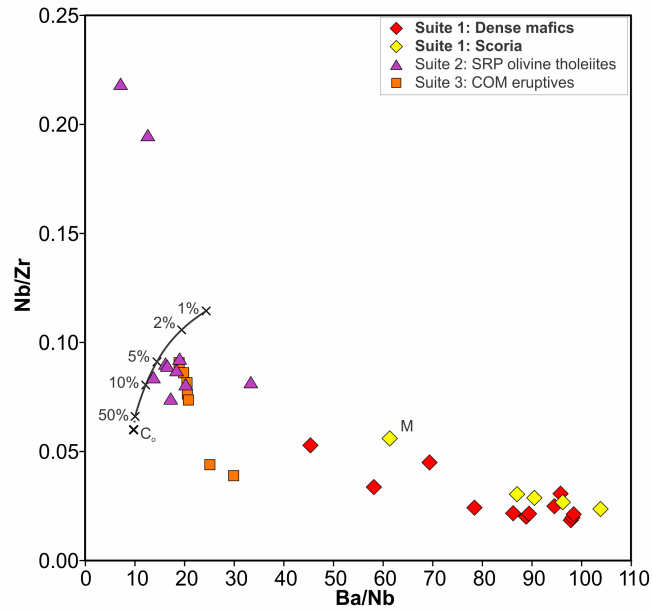
(a)

data-point error ellipses are 2se

Age = 2770±520 Ma
MSWD = 973

(b)

data-point error ellipses are 2se
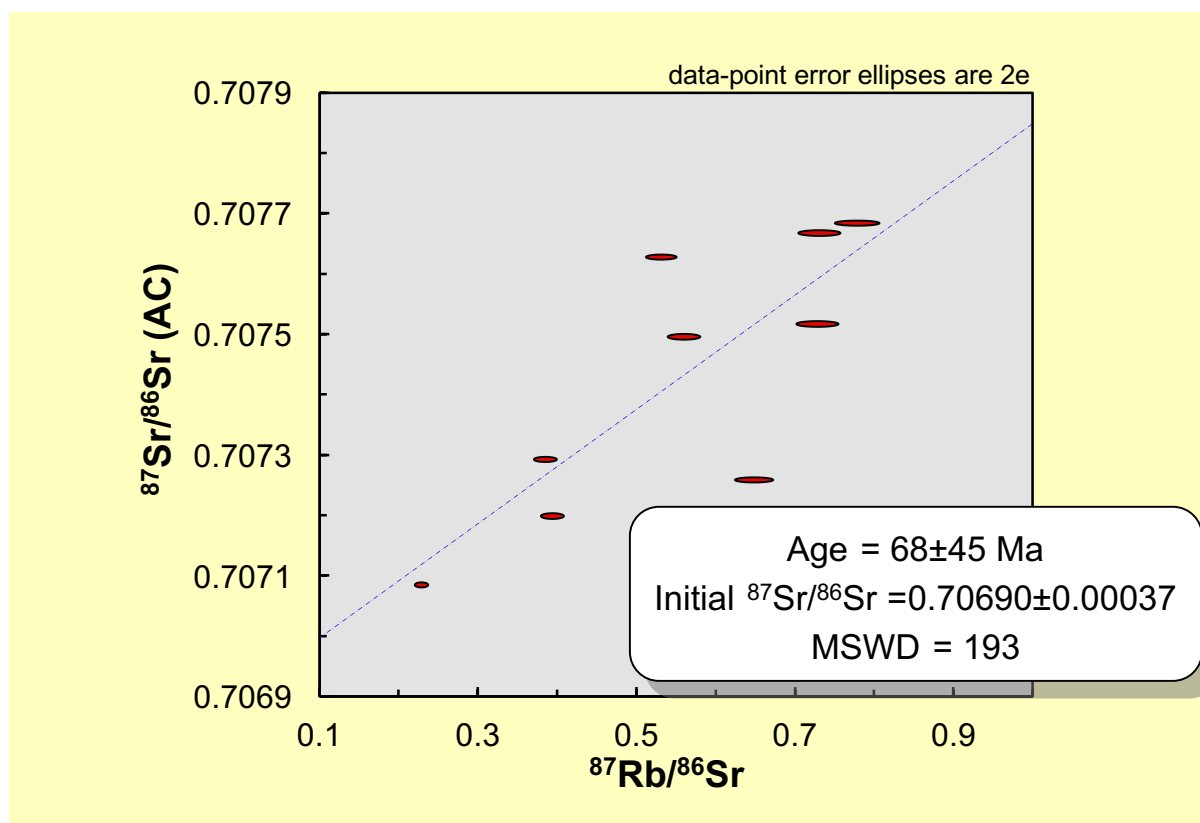
Age = 2995±220 Ma
MSWD = 4.1

Supplemental Fig. 5: Pb-Pb isochrons generated using Isoplot (Ludwig 2008) for (a) Suite 2 samples (olivine tholeiites), (b) Suite 1 HRT mafics (minus YP122) and (c) Suite 3 Craters of the Moon samples. Ellipses represent 2se errors.
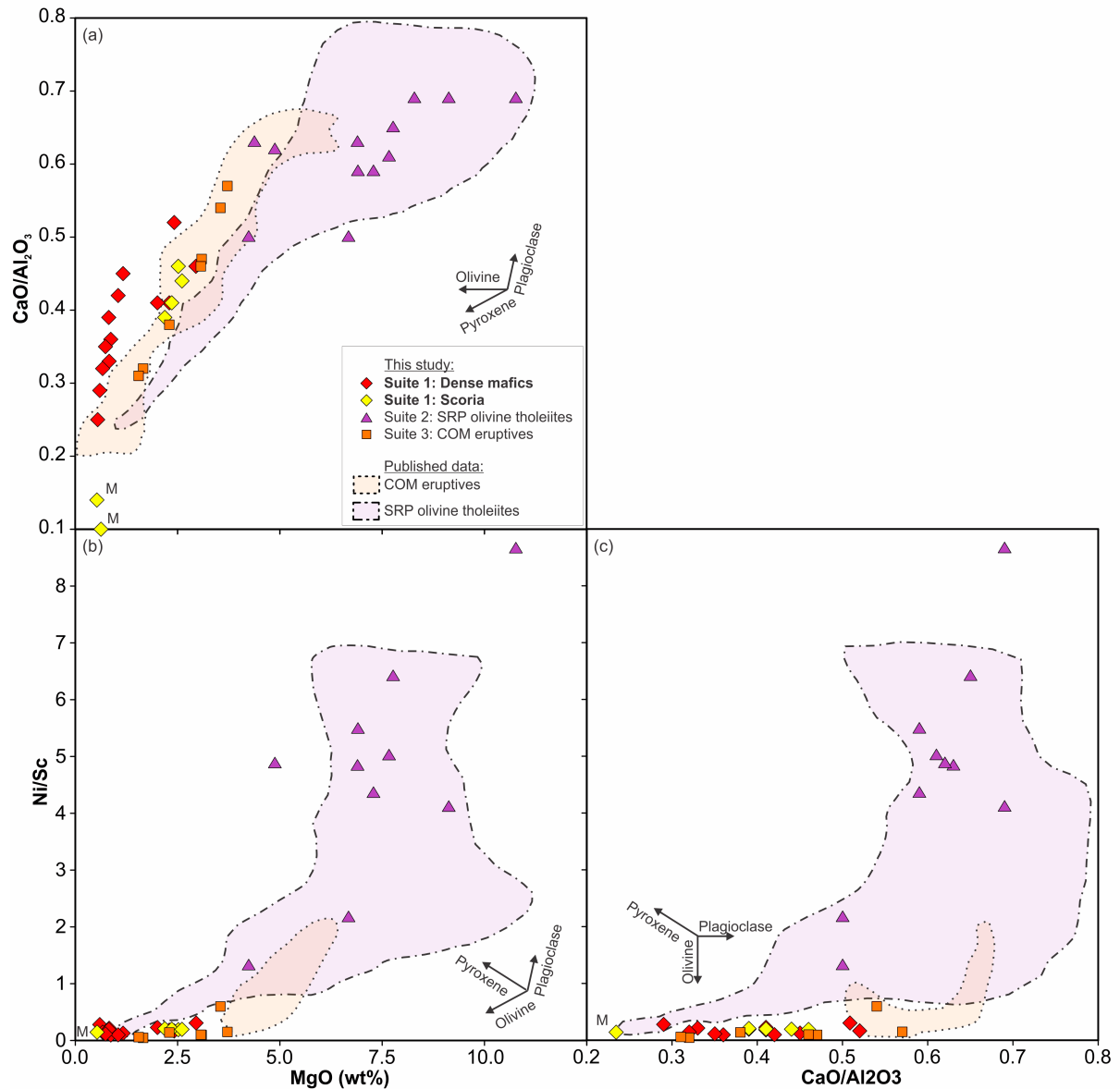
Supplemental Fig. 6: Ba/Nb vs. Nb/Zr for all suites in this study. Incompatible element ratios are sensitive to variations in the degree of partial melting of a common source. Curved line explores changes in the ratios with different degrees of partial melting of a primitive mantle source with composition C_o (McDonough and Sun 1989). Partition coefficients of 0.01, 0.04 and 0.08 for D_{Ba}, D_{Nb} and D_{Zr}, respectively (Hofmann 1988). Although the absolute values are approximates, the relative compatibilities are the controlling factor on the trends. The trends show that it is unlikely the different suites can be explained through different degrees of partial melting of a common source zone. Batch melting was modeled using the equation:

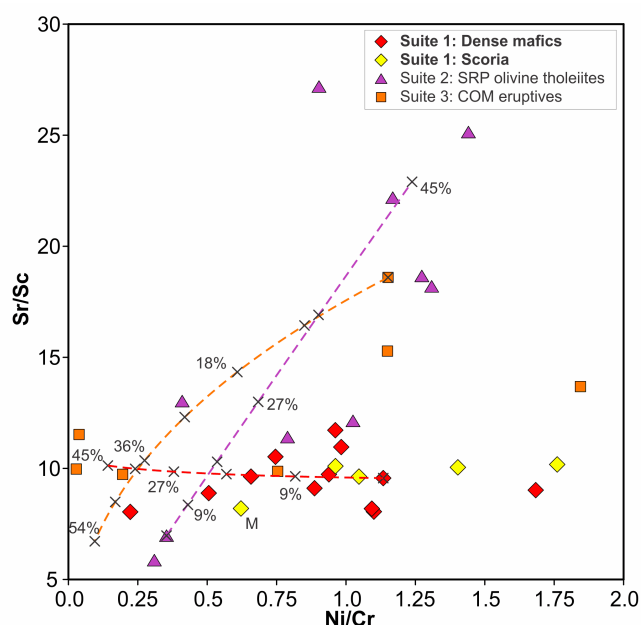$$\frac{C_L}{C_O} = \frac{1}{\overline{D}(1 - F) + F}$$

where C_L and C_O are the liquid and original concentrations respectively, F is the fraction of melt [melt/(melt+rock)] and $\overline{D}$ is the bulk elemental distribution coefficient.

Supplemental Fig. 7: Sr isotope isochron generated using Isoplot (Ludwig 2008) for the HRT mafics suite. Ratios were age-corrected using an age of 2.08 Ma (Rivera et al. 2014; Wotzlaw et al. 2015). Ellipses represent 2se ($^{87}Sr/^{86}Sr$) and 3% ($^{87}Rb/^{86}Sr$) errors. The imprecise late Cretaceous age coincides with widespread volcanism in the western US (Christiansen and Yeats 1992) and is consistent with the young metasomatic event inferred in the Absaroka volcanic province by Feeley (2003) and from Wyoming lamproites by Mirnejad and Bell (2006). The initial $^{87}Sr/^{86}Sr$ value of 0.7069 is similar to the focus of Yellowstone-Snake River Plain basalts (McCurry and Rodgers 2009).

Supplemental Fig. 8: Plots showing the relationship between MgO, CaO/Al_2O_3 and Ni/Sc, showing intra-suite variation (see text in the main paper for sources of published data). Arrows indicate the trend of melt evolution as a result of crystallization of the three principal phases in comparable rocks. These plots indicate that Suite 2 variation is compatible with olivine and pyroxene crystallization whereas the trends in Suites 1 and 3 suggest a lesser role for olivine.

Supplemental Fig. 9: Ni/Cr vs. Sr/Sc ratios for the samples analyzed in this study. Red, purple and orange dashed lines show modeled fractional crystallization trends for Suite 1 (YP122 as a starting composition, crystallizing 45% plagioclase, 30% olivine and 25% clinopyroxene), Suite 2 (YR291 as starting composition, crystallizing assemblage of 60% clinopyroxene, 35% olivine, 5% plagioclase) and Suite 3 (YR422 as starting composition, crystallizing assemblage of 80% plagioclase, 15% olivine, 5% clinopyroxene), respectively (see text for details). Modeling was done using the modeler from Ersoy and Helvaci (2010). Black crosses represent 9% increments of crystallization. The positive correlation in Suite 2 samples is consistent with a clinopyroxene-olivine dominated crystallizing assemblage in contrast to a decrease in Sr/Sc with fractionation in Suite 3 samples, consistent with a plagioclase-dominant assemblage due to the compatible nature Sc and Sr in clinopyroxene and plagioclase, respectively. The uniform Sr/Sc with decreasing Ni/Cr is consistent with a more balanced assemblage.

Isotope methodologies

Separation of Sr, Nd and Pb were achieved through extraction chromatography based on the method of Pin et al. (2014). Two aliquots of rock powder, one for Sr and Nd, and one for Pb (containing ≥300 ng Pb) of rock powder were digested in pre-cleaned Savillex screw-topped Teflon beakers using a combination of HF, HNO_3 and HCl. The Sr and Nd digested sample was taken up in 6M HNO_3 ready to pass through cleaned columns loaded with pre-cleaned Sr-Spec resin. The Sr-Spec resin was pre-conditioned with ~0.5 ml 9M HNO_3. The sample was loaded and then washed sequentially with 100, 200, and 3 x 1000 µl 9M HNO_3 to remove Ba and other unwanted elements. The wash was collected for further separation to extract Nd. 2 ml 0.05 M HNO_3 was then passed through the Sr-Spec column to collect the Sr.

The dried Nd fraction was taken up with 1ml of 1 M HNO_3 containing 50 mg ml^{-1} ascorbic acid ($C_6H_8O_6$) in order to reduce the $Fe_{(III)}$ present. This nitric and ascorbic solution was previously passed through a TRU-Spec column in order to reduce the Nd procedural blank. When the sample solution turned pale-yellow the solution was ready to pass through the columns.

The TRU-Spec columns were pre-conditioned with 0.25 ml of the HNO_3-ascorbic solution before addition of the sample solution. Then 50, 100, 200 and 2 x 1000 µl of 1M HNO_3 was passed through the column to remove all unwanted elements. Then the LREE, Th and U fraction was removed and collected through addition of 2 x 1 ml of 0.05 HNO_3. This eluted fraction was then dried and taken up with 300 µl 0.25 M HCl and put through the LN-Spec column. The lanthanides were sequentially eluted through further addition of 0.25 M HCl. Column calibrations were undertaken to identify the Nd fraction and to minimize Ce and Pr overlap. This specified collection after the addition of 8 ml 0.25 M HCl and collection for a further 4 ml. This fraction was free of Sm.

The dried Pb digestion was taken up in 0.5 ml 1M HBr. This was passed through AG1-X8 anion resin. The pre-cleaned resin was further cleaned by passing alternating MQ water and 6M HCl through the resin twice. Any residual HCl was then washed out through the passing of ~ 2.5 ml MQ through the resin. The resin was then pre-conditioned with 0.5 ml 1M HBr before the sample was loaded. The sample was then eluted with two passes of 0.5 ml 1M HBr. Pb was then collected with two 0.5 ml washes of 6M HCl. This entire process was repeated. Prior to drying, ~0.1 ml conc. HNO_3 was added to the collected solution to ensure the evaporation of all remaining Br.

Isotope analyses were run on a ThermoFisher Triton Thermal Ionization Mass spectrometer (TIMS) at the Open University, UK and Victoria University of Wellington, New Zealand on the same instrument.

The dried Sr fraction was dissolved in concentrated HNO_3 with a ratio of ~1 μl to 1000 ng Sr. 0.7 μl of pre-cleaned TaF_2 activator (as in Charlier et al. 2006) was loaded onto a single Re filament. Before the activator had dried, 1 μl of the sample was added to ensure the load was mixed on the filament. Filaments were heated sufficiently (1450-1500 °C) to generate ~50 mV ^{84}Sr. 240 ratios were measured in blocks of 10. A peak-center and tune was automated at the beginning of every 10 blocks.

The dried Nd fraction was taken up in 1-2 μl conc. HCl until dissolved. 200-800 ng of the sample was loaded onto a double Re filament following the addition, and drying, of 1 μl H_3PO_4 loading solution. A further 1 μl of loading solution was added following evaporation of the sample solution and then dried.

Nd was run using a double filament assembly with an evaporation filament (containing the sample) and a hotter ionization filament (1650-1800 °C) to generate 2-8 V ^{142}Nd depending on the size of the sample. 270 ratios were analyzed in blocks with a peak-

center and tune completed prior to every 10 blocks. Time-corrected mass dependent fractionation of the ^{143}Nd/^{144}Nd ratios was corrected for using an exponential law and normalization to ^{146}Nd/^{144}Nd = 0.7219.

The dried Pb fraction was taken up in 2 µl H_3PO_4-silica gel mix (Gerstenberger and Haase 1996). Half was loaded onto a single Re filament and run naturally for 180 ratios (integration time of 8.389 s). The remaining aliquot was then mixed outside of the beaker with a ^{207}Pb/^{204}Pb spike (Thirlwall 2000). Spiked aliquots were then loaded onto single Re filaments and analyzed for 120 ratios under the same conditions. The data was then deconvolved to determine the isotopic ratios.

References cited

Charlier, B.L.A., Ginibre, C., Morgan, D., Nowell, G.M., Pearson, D.G., Davidson, J.P., and Ottley, C.J. (2006) Methods for the microsampling and high-precision analysis of strontium and rubidium isotopes at single crystal scale for petrological and geochronological applications. Chemical Geology, 232, 114-133.

Christiansen, R.L., and Yeats, R.S. (1992) Post-Laramide geology of the U.S. Cordilleran region. In B.C. Burchfield, P.W. Lipman, and M.L. Zoback, Eds., The Cordilleran orogeny: conterminous U.S., The Geology of North America, G-3, 261-406. Geological Society of America, Boulder, Colorado.

Ersoy, Y., and Helvaci, C. (2010) FC-AFC-FCA and mixing modeler: a Microsoft® Excel© spreadsheet program for modeling geochemical differentiation of magma by crystal fractionation, crustal assimilation and mixing. Computers & Geosciences, 36, 383-390.

Feeley, T.C. (2003) Origin and tectonic implications of across-strike geochemical variations in the Eocene Absaroka volcanic province, United States. Journal of Geology, 111, 329-346.

Gerstenberger, H., and Haase, G. (1996) A highly effective emitter substance for mass spectrometric Pb isotope ratio determinations. Chemical Geology, 136, 309-312.

Hofmann, A.W. (1988) Chemical differentiation of the Earth: the relationship between mantle, continental crust, and oceanic crust. Earth and Planetary Science Letters, 90, 297-314.

Jochum, K.P., Weis, U., Schwager, B., Stoll, B., Wilson, S.A., Haug, G.H., Andreae, M.O., and Enzweiler, J. (2016) Reference values following ISO guidelines for frequently requested rock reference materials. Geostandards and Geoanalytical Research, 40, 333-350.

Ludwig, K.R. (2008) Isoplot/Ex version 3.70, A geochronological toolkit for Microsoft Excel, revision of August 26, 2008. Berkeley Geochronology Center Special Publication 4.

McCurry, M., and Rodgers, D.W. (2009) Mass transfer along the Yellowstone hotspot track I: Petrologic constraints on the volume of mantle-derived magma. Journal of Volcanology and Geothermal Research, 188, 86-98.

McDonough, W.F., and Sun, S.-s. (1995) The composition of the Earth. Chemical Geology, 120, 223-253.

Mirnejad, H., and Bell, K. (2006) Origin and source evolution of the Leucite Hills lamproites: evidence from Sr-Nd-Pb-O isotopic compositions. Journal of Petrology, 47, 2463-2489.

Pin, C., Gannoun, A., and Dupont, A. (2014) Rapid, simultaneous separation of Sr, Pb, and Nd by extraction chromatography prior to isotope ratios determination by TIMS and MC-ICP-MS. Journal of Analytical Atomic Spectrometry, 29, 1858-1870.

Rivera, T.A., Schmitz, M.D., Crowley, J.L., and Storey, M. (2014) Rapid magma evolution constrained by zircon petrochronology and ^{40}Ar/^{39}Ar sanidine ages for the Huckleberry Ridge Tuff, Yellowstone, USA. Geology, 42, 643-646.

Thirlwall, M.F. (2000) Inter-laboratory and other errors in Pb isotope analyses investigated using a ^{207}Pb-^{204}Pb double spike. Chemical Geology, 163, 299-322.

Wotzlaw, J.-F., Bindeman, I.N., Stern, R.A., D'Abzac, F.-X., and Schaltegger, U. (2015) Rapid heterogeneous assembly of multiple magma reservoirs prior to Yellowstone supereruptions. Scientific Reports, 5, 14026.

Electronic appendix captions

Electronic appendix 1: Full major and trace elemental concentrations (major element oxides in wt%, trace element concentrations in ppm), and isotopic ratios for the samples analyzed in this study. Averages of reference materials analyzed by XRF and ICP-MS are also documented along with 2sd variation. Reference values from Jochum et al. (2016).

Electronic appendix 2: Table of published data from GEOROC database (http://georoc.mpch-mainz.gwdg.de/georoc/), which met compositional criteria, to explore possible end-members for crustal assimilation.